Breaking the current density threshold in spin-orbit-torque magnetic random access memory

Yin Zhang,[1,2] H. Y. Yuan,[3,*] X. S. Wang,[1,4] and X. R. Wang[1,2,†]

[1]*Physics Department, The Hong Kong University of Science and Technology, Clear Water Bay, Kowloon, Hong Kong*

[2]*HKUST Shenzhen Research Institute, Shenzhen 518057, China*

[3]*Department of Physics, Southern University of Science and Technology, Shenzhen 518055, China*

[4]*School of Microelectronics and Solid-State Electronics, University of Electronic Science and Technology of China, Chengdu, Sichuan 610054, China*

(Received 26 December 2017; revised manuscript received 7 February 2018; published 20 April 2018)

Spin-orbit-torque magnetic random access memory (SOT-MRAM) is a promising technology for the next generation of data storage devices. The main bottleneck of this technology is the high reversal current density threshold. This outstanding problem is now solved by a new strategy in which the magnitude of the driven current density is fixed while the current direction varies with time. The theoretical limit of minimal reversal current density is only a fraction (the Gilbert damping coefficient) of the threshold current density of the conventional strategy. The Euler-Lagrange equation for the fastest magnetization reversal path and the optimal current pulse is derived for an arbitrary magnetic cell and arbitrary spin-orbit torque. The theoretical limit of minimal reversal current density and current density for a GHz switching rate of the new reversal strategy for CoFeB/Ta SOT-MRAMs are, respectively, of the order of 10^5 A/cm^2 and 10^6 A/cm^2 far below 10^7 A/cm^2 and 10^8 A/cm^2 in the conventional strategy. Furthermore, no external magnetic field is needed for a deterministic reversal in the new strategy.

DOI: 10.1103/PhysRevB.97.144416

I. INTRODUCTION

Fast and efficient magnetization reversal is not only fundamentally interesting, but also technologically important for high-density data storage and massive information processing. Magnetization reversal can be induced by a magnetic field [1–3], by an electric current through direct [4–9] and/or indirect [10–22] spin angular momentum transfer from polarized itinerant electrons to magnetization, by a microwave [23], by a laser light [24], or even by an electric field [25]. While the magnetic-field-induced magnetization reversal is a mature technology, it suffers from scalability and field localization problems [8,26] for nanoscale devices. Spin-transfer-torque magnetic random access memory is an attractive technology in spintronics [26] although Joule heating, device durability, and reliability are challenging issues [11,26]. In a spin-orbit-torque magnetic random access memory (SOT-MRAM) whose central component is a heavy-metal/ferromagnet bilayer, an electric current in the heavy-metal layer generates a pure spin current through the spin-Hall effect [10,11] that flows perpendicularly into the magnetic layer. The spin current, in turn, produces spin-orbit torques (SOTs) through spin angular momentum transfer [4,5] and/or Rashba effect [16–22]. SOT-MRAM is a promising technology because writing charge current does not pass through the memory cells so that the cells do not suffer from the Joule heating and associated device damaging. In principle, such devices are infinitely durable due to negligible heating from spin current [11]. However, the reversal current density threshold (above 10^7 A/cm^2 [14,15] for realistic materials) in the present SOT-MRAM architecture is too high. To have a reasonable switching rate (order of GHz), the current density should be much larger than 10^8 A/cm^2 [14,15], which is too high for devices. In order to lower the minimal reversal current density as well as to switch magnetization states at GHz rate at a tolerable current density in SOT-MRAM, it is interesting to find new reversal schemes (strategies) that can achieve the above goals. In this paper, we show that a proper current density pulse of time-dependent flow direction and constant magnitude, much lower than the conventional threshold, can switch a SOT-MRAM at GHz rate. Such a time-dependent current pulse can be realized by using two perpendicular currents passing through the heavy-metal layer. The theoretical limit of minimal reversal current density of the new reversal strategy for realistic materials can be of the order of 10^5 A/cm^2, far below 10^7 A/cm^2 in the conventional strategy that uses a direct current (dc), both based on macrospin approximation. The validity of the macrospin model is also verified by micromagnetic simulations.

II. MACROSPIN MODEL AND RESULTS

A. Model

Our SOT-MRAM model consists of a ferromagnetic/heavy-metal bilayer lying in the $x'y'$ plane, as shown in Fig. 1(a). In the absence of an electric current, the system has two stable states $\mathbf{m} = \mathbf{m}_0$ and $\mathbf{m} = -\mathbf{m}_0$ where $\mathbf{m}$ is the unit direction of magnetization $\mathbf{M} = M\mathbf{m}$ of magnitude M. An xyz coordinate is defined in Fig. 1(b) where the z axis is along $\mathbf{m}_0$ and the y axis is in the $x'y'$ plane. θ_0 and ϕ_0 are the polar and azimuthal angles of $\mathbf{m}_0$ in the $x'y'z'$ coordinate. Two time-dependent electric currents flow along the $+x'$ and $+y'$ directions such that the magnitudes of the total current density J is a constant. Thus the electric current density vector is $\mathbf{J} = J\cos\Phi\hat{x}' +$

*Corresponding author: yuanhy@sustc.edu.cn

†Corresponding author: phxwan@ust.hk

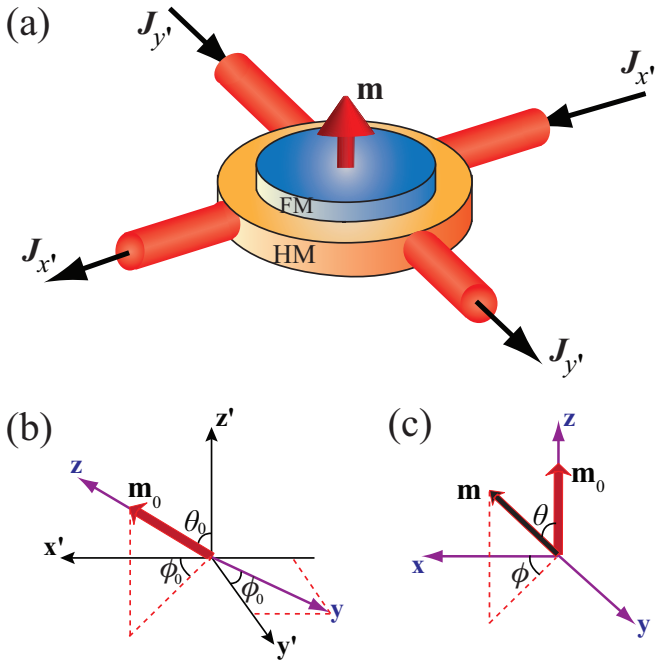

FIG. 1. (a) Schematic illustration of new reversal scheme for SOT-MRAMs. Two perpendicular currents flow in the heavy-metal layer of a ferromagnet/heavy-metal bilayer to generate a current whose direction can vary in the $x'y'$ plane. (b) and (c) Definitions of coordinates. The x' and y' axes are the two currents flow directions in the heavy-metal layer. The xyz is a moving coordinate with the z axis along $\mathbf{M}_0$, and the y axis in the $x'y'$ plane. θ_0 and ϕ_0 are the polar and azimuthal angles of $\mathbf{M}_0$ in the $x'y'z'$ coordinate, while θ and ϕ are the polar and azimuthal angles of $\mathbf{M}$ in the xyz coordinate.

$J \sin\Phi \hat{y}'$, here Φ is a time-dependent angle between $\mathbf{J}$ and the x' axis. The electric current generates a transverse spin current perpendicularly flowing into the ferromagnetic layer via the spin-Hall effect [10], and then produces an effective SOT on the magnetization [4,5,16], i.e.,

$$\vec{\tau} = -a\mathbf{m} \times (\mathbf{m} \times \hat{s}) + \beta a \mathbf{m} \times \hat{s}, \tag{1}$$

where the first term on the right-hand side is the Slonczewski-like torque while the second term is the fieldlike torque. The spin-polarization direction is $\hat{s} = \hat{J} \times \hat{z}'$ (for other type of spin-Hall effect, see Ref. [27]) with $\hat{J}$ being the unit vector of current density. $a = \frac{\hbar}{2ed}\theta_{\rm SH} J$ is proportional to J where $\hbar$, e, and d are respectively the Plank constant, the electron charge, and the sample thickness. $\theta_{\rm SH}$ is the spin Hall angle, which measures the conversion efficiency between the spin current and charge current. β measures the fieldlike torque and can be an arbitrary real number since this torque may also be directly generated from the Rashba effect [16].

The magnetization dynamics under an in-plane current density $\mathbf{J}$ is governed by the generalized dimensionless Landau-Lifshitz-Gilbert (LLG) equation,

$$\frac{\partial \mathbf{m}}{\partial t} = -\mathbf{m} \times \mathbf{h}_{\rm eff} + \alpha \mathbf{m} \times \frac{\partial \mathbf{m}}{\partial t} + \vec{\tau}, \tag{2}$$

where α is the Gilbert damping constant that is typically much smaller than unity. The effective field is $\mathbf{h}_{\rm eff} = -\nabla_{\mathbf{m}}\varepsilon$ from energy density ε. Time, magnetic field, and energy density are respectively in units of $(\gamma M)^{-1}$, M, and $\mu_0 M^2$, where γ and μ_0 are, respectively, the gyromagnetic ratio and vacuum magnetic permeability. In this unit system, $a = \frac{\hbar}{2ed\mu_0 M^2}\theta_{\rm SH} J$ becomes dimensionless.

The magnetization $\mathbf{m}$ can be conveniently described by a polar angle θ and an azimuthal angle ϕ in the xyz coordinate [shown in Fig. 1(c)]. In terms of θ and ϕ, the generalized LLG equation (2) becomes

$$(1+\alpha^2)\dot{\theta} = h_{{\rm eff},\phi} + a s_\theta - \beta a s_\phi + \alpha(h_{{\rm eff},\theta} - a s_\phi - \beta a s_\theta) \equiv F_1, \tag{3a}$$

$$(1+\alpha^2)\dot{\phi}\sin\theta = -h_{{\rm eff},\theta} + a s_\phi + \beta a s_\theta + \alpha(h_{{\rm eff},\phi} + a s_\theta - \beta a s_\phi) \equiv F_2, \tag{3b}$$

where $h_{{\rm eff},\theta} = \frac{\partial \varepsilon}{\partial \theta}$, $h_{{\rm eff},\phi} = -\frac{\partial \varepsilon}{\partial \phi}$, and s_θ and s_ϕ are

$$s_\theta = \cos\theta_0 \sin(\Phi - \phi_0)\cos\theta\cos\phi - \cos(\Phi - \phi_0)\cos\theta\sin\phi - \sin\theta_0 \sin(\Phi - \phi_0)\sin\theta,$$

$$s_\phi = -\cos\theta_0 \sin(\Phi - \phi_0)\sin\phi - \cos(\Phi - \phi_0)\cos\phi.$$

B. Derivation of the Euler-Lagrange equation

The goal is to reverse the initial state $\theta = 0$ ($\mathbf{m} = \mathbf{m}_0$) to the target state $\theta = \pi$ ($\mathbf{m} = -\mathbf{m}_0$) by SOT. There are an infinite number of paths that connect the initial state $\theta = 0$ with the target state $\theta = \pi$, and each of these paths can be used as a magnetization reversal route. For a given reversal route, there are an infinite number of current pulses that can reverse the magnetization. The theoretical limit of minimal current density J_c is defined as the smallest values of minimal reversal current densities of all possible reversal routes. Then come two interesting and important questions: (i) What is J_c above which there is at least one reversal route that the current density can reverse the magnetization along it? (ii) For a given $J > J_c$, what are the optimal reversal route and the optimal current pulse $\Phi(t)$ that can reverse the magnetization at the highest speed?

Dividing Eq. (3b) by Eq. (3a), one can obtain the following constraint,

$$G \equiv \frac{\partial \phi}{\partial \theta}\sin\theta F_1 - F_2 = 0. \tag{4}$$

The magnetization reversal time T is

$$T = \int_0^\pi \frac{d\theta}{\dot{\theta}} = \int_0^\pi \frac{1+\alpha^2}{F_1} d\theta. \tag{5}$$

The optimization problem here is to find the optimal reversal route $\phi(\theta)$ and the optimal current pulse $\Phi(t)$ such that T is minimum under constraint (4). Using the Lagrange multiplier method, the optimal reversal route and the optimal current pulse satisfy the Euler-Lagrange equations [28,29],

$$\frac{\partial F}{\partial \phi} = \frac{d}{d\theta}\left(\frac{\partial F}{\partial(\partial\phi/\partial\theta)}\right), \frac{\partial F}{\partial \Phi} = \frac{d}{d\theta}\left(\frac{\partial F}{\partial(\partial\Phi/\partial\theta)}\right), \tag{6}$$

where $F = (1+\alpha^2)/F_1 + \lambda G$ and λ is the Lagrange multipliers, which can be determined self-consistently by Eq. (6) and constrain (4). Given a current density of constant magnitude J, Eq. (6) may or may not have a solution of $\phi(\theta)$ that

continuously passing through $\theta = 0$ and $\theta = \pi$. If such a solution exists, then $\phi(\theta)$ is the optimal path for the fastest magnetization reversal and the corresponding solution of $\Phi(t)$ is the optimal current pulse. The theoretical limit of minimal reversal current density is then the smallest current density J_c below which the optimal reversal path does not exist.

C. Optimal current pulse and theoretical limit of minimal reversal current density

As an example, we consider a uniaxial system with the easy axis along the z' axis so that xyz and $x'y'z'$ coordinates are the same and $\varepsilon = -K\cos^2\theta$ where K is the anisotropy coefficient. This is the case of many recent experiments [13,14,18]. Thus, we have $F_1 = -\alpha K \sin 2\theta + a(1-\alpha\beta)\cos\theta\sin(\Phi_J - \phi) + a(\alpha+\beta)\cos(\Phi_J - \phi)$, $F_2 = K\sin 2\theta - a(1-\alpha\beta)\cos(\Phi_J - \phi) + a(\alpha+\beta)\cos\theta\sin(\Phi_J - \phi)$, and $G = (\partial\phi/\partial\theta)\sin\theta F_1 - F_2$. Obviously, $\frac{\partial F_1}{\partial\phi} = -\frac{\partial F_1}{\partial\Phi}$, $\frac{\partial F_2}{\partial\phi} = -\frac{\partial F_2}{\partial\Phi}$, and $\frac{\partial G}{\partial\phi} = -\frac{\partial G}{\partial\Phi}$. Then the Euler-Lagrange equation of (6) becomes

$$\lambda\frac{d}{d\theta}(F_1\sin\theta) = 0, \tag{7a}$$

$$\frac{1+\alpha^2}{F_1^2}\frac{\partial F_1}{\partial\phi} - \lambda\frac{\partial G}{\partial\phi} = -\frac{1+\alpha^2}{F_1^2}\frac{\partial F_1}{\partial\Phi} + \lambda\frac{\partial G}{\partial\Phi} = 0. \tag{7b}$$

From Eq. (7a), one has $\lambda \neq 0$ or $\lambda = 0$. If $\lambda \neq 0$, F_1 must be $F_1 = C/\sin\theta$ ($C \neq 0$) so that $(1+\alpha^2)\dot\theta = C/\sin\theta \to \infty$ as $\theta \to 0$ or π. This solution is not physical, and should be discarded. Therefore, the only allowed solution must be $\lambda = 0$, and one has $\partial F_1/\partial\Phi = 0$ according to Eq. (7b). Interestingly, this is exactly the condition of maximal $\dot\theta = F_1/(1+\alpha^2)$ as Φ varies. Φ satisfies $\tan(\Phi-\phi) = \frac{1-\alpha\beta}{\alpha+\beta}\cos\theta$, or

$$\Phi = \tan^{-1}\left(\frac{1-\alpha\beta}{\alpha+\beta}\cos\theta\right) + \phi + \pi \quad (\beta < -\alpha) \tag{8a}$$

$$\Phi = \tan^{-1}\left(\frac{1-\alpha\beta}{\alpha+\beta}\cos\theta\right) + \phi \quad (\beta > -\alpha). \tag{8b}$$

Substituting Eq. (8) into the LLG equation (3), $\theta(t)$ and $\phi(t)$ are determined by the following equations:

$$\dot\theta = \frac{1}{1+\alpha^2}[aP(\theta) - \alpha K\sin 2\theta], \tag{9a}$$

$$\dot\phi = \frac{1}{1+\alpha^2}\left[2K\cos\theta - a(\alpha+\beta)(1-\alpha\beta)\frac{\sin\theta}{P(\theta)}\right], \tag{9b}$$

where $P(\theta) = \sqrt{(\alpha+\beta)^2 + (1-\alpha\beta)^2\cos^2\theta}$. To reverse magnetization from $\theta = 0$ to $\theta = \pi$, a must satisfy $a > \alpha K\sin(2\theta)/P(\theta)$ according to Eq. (9a) so that $\dot\theta$ is no negative for all θ. Obviously, $\dot\theta = 0$ at $\theta = \pi/2$ when $\beta = -\alpha$. The magnetization reversal is not possible in this case, and $\beta = -\alpha$ is a singular point. The theoretical limit of minimal reversal current density J_c for $\beta \neq -\alpha$ is

$$J_c = \frac{2\alpha e K d}{\theta_{\rm SH}\hbar}Q, \tag{10}$$

where $Q \equiv \max\{\sin 2\theta/P(\theta)\}$ for $\theta \in [0,\pi]$.

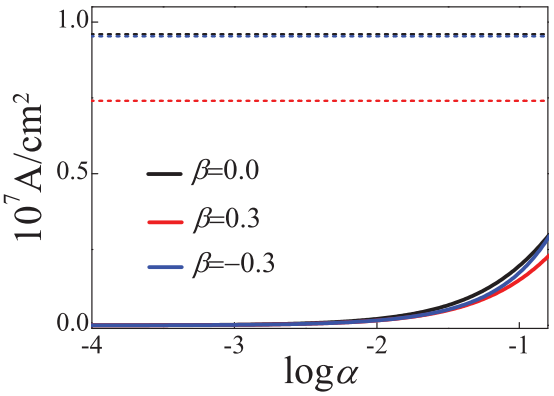

FIG. 2. The $\log\alpha$ dependence of J_c for various β are plotted as the solid curves for model parameters of $M = 3.7\times10^5$ A/m, $K = 5.0\times10^3$ J/m^3, $\theta_{\rm SH} = 0.084$, and $d = 0.6$ nm. As a comparison, $J_c^{\rm dc}$ is also plotted as the dashed lines.

In comparison with the current density threshold [13,14,18] ($J_c^{\rm dc}$) in the conventional strategy for $\beta = 0$,

$$J_c^{\rm dc} = \frac{2eKd}{\theta_{\rm SH}\hbar}\left(1 - \frac{H}{\sqrt{2}K}\right), \tag{11}$$

the minimal reversal current density is reduced by more than a factor of α. Here H ($\simeq 22$ Oe in experiments [15]) is a small external magnetic needed for a deterministic reversal in conventional strategy. Using CoFeB/Ta parameters of $M = 3.7\times10^5$ A/m, $K = 5.0\times10^3$ J/m^3, $\theta_{\rm SH} = 0.084$, and $d = 0.6$ nm [11,14,15], Fig. 2 shows $\log\alpha$ dependence of J_c (solid lines) and $J_c^{\rm dc}$ (dashed lines) for $\beta = 0$ (black), 0.3 (red), and -0.3 (blue), respectively. Both $J_c^{\rm dc}$ and J_c depend on β. The lower the damping of a magnetic material is, the smaller our minimum switching current density will be. For a magnetic material of $\alpha = 10^{-5}$, the theoretical limit of minimal reversal current density can be five orders of magnitude smaller than the value in the conventional strategy.

For a given $J > J_c$, the shortest reversal time is given by Eqs. (5) and (9a):

$$T = \int_0^\pi \frac{1+\alpha^2}{aP(\theta) - \alpha K\sin 2\theta}d\theta. \tag{12}$$

The optimal reversal path is given by $\phi(\theta) = \int_0^\theta \frac{\dot\phi}{\dot\theta}d\theta'$ where $\dot\theta$ and $\dot\phi$ are given by Eqs. (9a) and (9b). Equation (9a) gives $t(\theta) = \int_0^\theta (1+\alpha^2)/[aP(\theta) - \alpha K\sin 2\theta]d\theta'$ and then $\theta(t)$ is just $\theta(t) = t^{-1}(\theta)$. Thus, $\Phi(\theta,\phi)$, $\phi(\theta)$ and $\theta(t)$ give $\phi(t) = \phi(\theta(t))$ and $\Phi(t) = \Phi(\theta(t),\phi(t))$. Using the same parameters as those for Fig. 2 with $\alpha = 0.008$ and various β, Figure 3 shows the optimal current pulses [Figs. 3(a)–3(c)] and the corresponding fastest magnetization reversal routes [Figs. 3(d)–3(f)] for $\beta = 0.3$ and $J = 1.92\times10^6$ A/cm^2 $\approx 15J_c$ [Figs. 3(a) and 3(d)], for $\beta = 0.1$ and $J = 9.0\times10^6$ A/cm^2 $\approx 58J_c$ [Figs. 3(b) and 3(e)], and for $\beta = 0.3$ and $J = 9.0\times10^6$ A/cm^2 $\approx 70J_c$ [Figs. 3(c) and 3(f)]. It is known that Ta has less effect on α [11]. The minimal reversal current density J_c under the optimal current pulse is 1.56×10^5 A/cm^2 for $\beta = 0.1$ and 1.28×10^5 A/cm^2 for $\beta = 0.3$, which

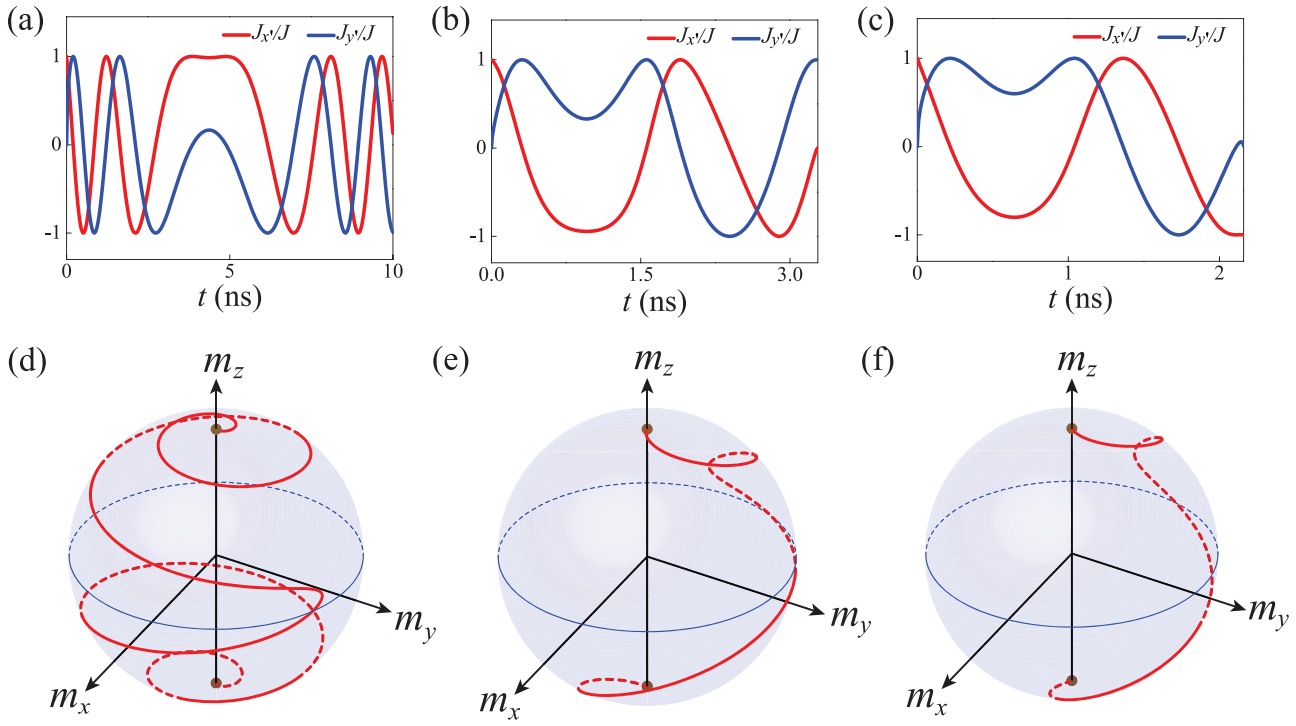

FIG. 3. Model parameters of $M = 3.7 \times 10^5$ A/m, $K = 5.0 \times 10^3$ J/m^3, $\theta_{\rm SH} = 0.084$, $\alpha = 0.008$, and $d = 0.6$ nm are used to mimic CoFeB/Ta bilayer, and $\beta = 0.3$ for (a), (c), (d), and (f) while $\beta = 0.1$ for (b) and (e). The theoretical limit of minimum reversal current density is $J_c = 1.56 \times 10^5$ A/cm^2 for $\beta = 0.1$ and $J_c = 1.28 \times 10^5$ A/cm^2 for $\beta = 0.3$. Optimal current pulses [(a)–(c)] and fastest reversal routes [(d)–(f)] are for $J = 1.92 \times 10^6$ A/cm^2 [(a) and (d)], and for $J = 9.0 \times 10^6$ A/cm^2 [(b), (c), (e), and (f)].

is far below $J_c^{\rm dc} = 9.6 \times 10^6$ A/cm^2 for the same material parameters [15]. The multiple oscillations of m_x and m_y reveal that the reversal is a spinning process and optimal reversal path winds around the two stable states many times. Correspondingly, the driving current makes also many turns as shown by the multiple oscillations of $J_{x'}$ and $J_{y'}$. The number of spinning turns depends on how far J is from J_c. The closer J to J_c is, the number of turns is larger. The number of turns is about five in Figs. 3(a) and 3(d) for $J \approx 15 J_c$ and one turn for $J > 50 J_c$ as shown in Figs. 3(b), 3(c), 3(e), and 3(f), so that the reversal is almost ballistic. The reversal time for $\beta = 0.3$ and $J = 1.92 \times 10^6$ A/cm^2 is about 10 nanoseconds, for $\beta = 0.1$ and $J = 9.0 \times 10^6$ A/cm^2 is about 3.3 nanoseconds, and for $\beta = 0.3$ and $J = 9.0 \times 10^6$ A/cm^2 is about 2.1 nanoseconds. Figure 4 is the reversal time T as a function of current density J under the optimal current pulse for the same parameters as those for Fig. 2. The reversal time quickly decreases to nanoseconds as current density increases. In a real experiment, there are many uncertainties so that the current pulse may be different from the optimal one. To check whether our strategy is robust against small fluctuations, we let the current pulse in Fig. 3(c) deviate from its exact value by as much as five percent. Numerical simulations show that these current pulses can still reverse the magnetization.

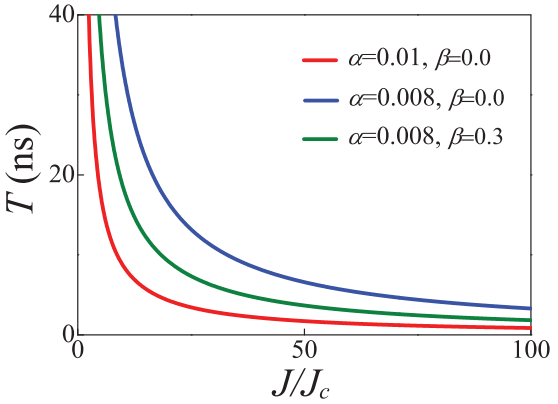

FIG. 4. Magnetization reversal time T under the optimal current pulses as a function of J for various α and β.

III. VERIFICATION OF MACROSPIN MODEL BY MICROMAGNETIC SIMULATION

In our analysis, the memory cell is treated as a macrospin. A natural question is how good the macrospin model is for a realistic memory device. To answer this question, we carried out micromagnetic simulations by using Newton-Raphson algorithm [30] for two memory cells of 150 nm × 150 nm × 0.6 nm [Figs. 5(a), 5(b) 5(d), and 5(e)] and 250 nm × 250 nm × 0.6 nm [Figs. 5(c) and 5(f)]. To model the possible edge pinning effect due to magnetic dipole-dipole interaction, we consider square-shape devices instead of a cylinder-shape device whose edge pinning is negligible. To make a quantitative comparison, the material parameters are the same as those used in Fig. 3. In our simulations, the exchange constant is $A = 1.3 \times 10^{-11}$ J/m to mimic CoFeB, and the unit cell size is 2 nm × 2 nm × 0.6 nm. For a fair comparison, the optimal

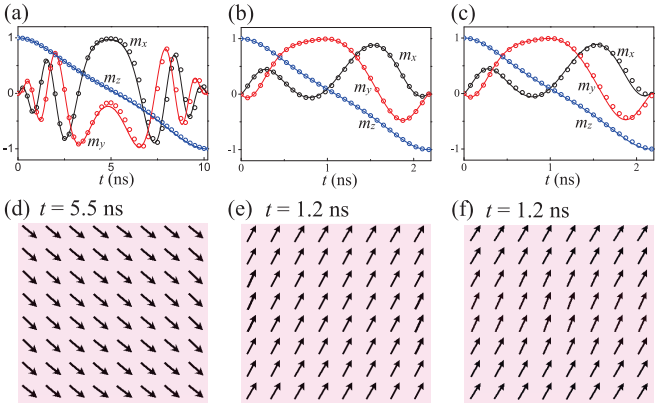

FIG. 5. (a)–(c) Time evolution of the average magnetization: cycles for micromagnetic simulations and solid lines are theoretical predictions from macrospin model. (a) and (b) are for the memory cell of 150 nm × 150 nm × 0.6 nm and optimal current pulse of current density of $J = 1.92 \times 10^6$ A/cm^2 and $J = 9.0 \times 10^6$ A/cm^2, respectively. (c) is for the memory cell of 250 nm × 250 nm × 0.6 nm and optimal current pulse of current density of $J = 9.0 \times 10^6$ A/cm^2. (d)–(f) Spin configurations respectively corresponding to (a)–(c) in the middle of magnetization reversal at $t = 5.5$ ns and 1.2 ns. The exchange constant is $A = 1.3 \times 10^{-11}$ J/m to mimic CoFeB, and the cell size in micromagnetic simulation is 2 nm × 2 nm × 0.6 nm.

current pulses shown in Figs. 3(a) and 3(c) of respective current density $J = 1.92 \times 10^6$ A/cm^2 and $J = 9.0 \times 10^6$ A/cm^2 were applied to the memory cell of 150 nm × 150 nm × 0.6 nm. The symbols in Figs. 5(a) and 5(b) are the time evolution of averaged magnetization m_x, m_y, and m_z while the solid lines are the theoretical predictions of macrospin model shown in Figs. 3(d) and 3(f). The perfect agreements prove the validity of the macrospin approximation for our device of such a size. To further verify that the memory device can be treated as a macrospin, Figs. 5(d) and 5(e) are the spin configurations in the middle of the reversal at $t = 5.5$ ns for Fig. 5(a) and at $t = 1.2$ ns for Fig. 5(b). The fact that all spins align almost in the same direction verifies the validity of the macrospin model. In real experiments, nonuniformity of current density is inevitable. To demonstrate the macrospin model is still valid, we let current density linearly vary from 9.5×10^6 A/cm^2 on the leftmost column of cells to 8.5×10^6 A/cm^2 on the rightmost column of cells. As expected, there is no noticeable difference with the data shown in Figs. 5(b) and 5(e).

For the large memory device of 250 nm × 250 nm × 0.6 nm, the optimal current pulse shown in Fig. 3(c) of current density $J = 9.0 \times 10^6$ A/cm^2 was considered. The time evolution of averaged magnetization m_x, m_y, and m_z are plotted in Fig. 5(c), with the symbols for simulations and solid lines for the macrospin model. They agree very well although there is a small deviation for a device of such a large size. Figure 5(f) is the spin configurations in the middle of the reversal at $t = 1.2$ ns for Fig. 5(c). The macrospin model is not too bad although all spins are not perfectly aligned. The slightly bent spin texture rotates coherently in this case.

In summary, for a normal SOT-MRAM device of size less than 300 nm [11,15], the macrospin model describes magnetization reversal well. However, for a larger sample size and lower current density ($J < 10^6$ A/cm^2 for the same material parameters as those used in Fig. 3), only the spins in the sample center can be reversed while the spins near the sample edges are pinned.

IV. DISCUSSION

Obviously, the strategy present here can easily be generalized to the existing spin-transfer-torque MRAM. The mathematics involved are very similar, and one expects a substantial current density reduction is possible there if a proper optimal current pulse is used. Of course, how to generate such a current pulse should be much more challenging than that for SOT-MRAM where two perpendicular currents can be used.

In the conventional strategy that uses a dc current, a static magnetic field along current flow is required for a deterministic magnetization reversal [13,14,18]. Although several field-free designs have been proposed [19,20], an antiferromagnet is needed to create an exchange bias, which plays the role of an applied magnetic field. As we have shown, such a requirement or complication is not needed in our strategy. Our strategy does not have another problem that exists in the conventional strategy in which the magnetization can only be placed near $\theta = \pi/2$ [13,14,18] so that the system falls into the target state by itself through the damping. Therefore, one would like to use materials with larger damping in the conventional strategy in order to speed up this falling process. In contrast, our strategy prefers low-damping materials, and reversal is almost ballistic when current density is large enough ($>50J_c$ in the current case). To reverse the magnetization from $\theta = \pi$ to $\theta = 0$, one only needs to reverse the current direction of the optimal current pulse. One should notice that the Euler-Lagrange equation allows us to easily obtain the optimal reversal current pulse and theoretical limit of the minimal reversal current density for an arbitrary magnetic cell such as in-plane magnetized layer [11] and biaxial anisotropy.

V. CONCLUSION

In conclusion, we investigated the magnetization reversal of SOT-MRAMs, and propose a new reversal strategy whose minimal reversal current density is far below the existing current density threshold. For the popular CoFeB/Ta system, it is possible to use a current density of the order of 10^6 A/cm^2 to reverse the magnetization at GHz rate, in comparison with order of $J \approx 10^8$ A/cm^2 in the conventional strategy.

ACKNOWLEDGMENTS

This work was supported by the National Natural Science Foundation of China (Grants No. 11774296 and No. 61704071) as well as Hong Kong RGC Grants No. 16300117 and No. 16301816. X.R.W. acknowledges the hospitality of Beijing Normal University and Beijing Computational Science Research Center during his visits.

[1] C. H. Back, R. Allenspach, W. Weber, S. S. P. Parkin, D. Weller, E. L. Garwin, and H. C. Siegmann, Science **285**, 864 (1999).

[2] M. Bauer, J. Fassbender, B. Hillebrands, and R. L. Stamps, Phys. Rev. B **61**, 3410 (2000).

[3] Z. Z. Sun and X. R. Wang, Phys. Rev. Lett. **97**, 077205 (2006).

[4] J. C. Slonczewski, J. Magn. Magn. Mater. **159**, L1 (1996).

[5] L. Berger, Phys. Rev. B **54**, 9353 (1996).

[6] J. A. Katine, F. J. Albert, R. A. Buhrman, E. B. Myers, and D. C. Ralph, Phys. Rev. Lett. **84**, 3149 (2000).

[7] Z. Li and S. Zhang, Phys. Rev. B **69**, 134416 (2004).

[8] W. Wetzels, G. E. W. Bauer, and O. N. Jouravlev, Phys. Rev. Lett. **96**, 127203 (2006).

[9] X. R. Wang and Z. Z. Sun, Phys. Rev. Lett. **98**, 077201 (2007).

[10] J. E. Hirsch, Phys. Rev. Lett. **83**, 1834 (1999).

[11] L. Liu, C.-F. Pai, Y. Li, H. W. Tseng, D. C. Ralph, and R. A. Buhrman, Science **336**, 555 (2012).

[12] S. Emori, U. Bauer, S.-M. Ahn, E. Martinez, and G. S. D. Beach, Nature Mater. **12**, 611 (2013).

[13] K.-S. Lee, S.-W. Lee, B.-C. Min, and K.-J. Lee, Appl. Phys. Lett. **102**, 112410 (2013).

[14] S. Fukami, T. Anekawa, C. Zhang, and H. Ohno, Nature Nanotech. **11**, 621 (2016).

[15] J.-Y. Chen, M. DC, Delin Zhang, Zhengyang Zhao, Mo Li, and J.-P. Wang, Appl. Phys. Lett. **111**, 012402 (2017).

[16] A. Manchon and S. Zhang, Phys. Rev. B **79**, 094422 (2009).

[17] I. M. Miron, G. Gaudin, S. Auffret, B. Rodmacq, A. Schuhl, S. Pizzini, J. Vogel, and P. Gambardella, Nature Mater. **9**, 230 (2010).

[18] X. Zhang, C. H. Wan, Z. H. Yuan, Q. T. Zhang, H. Wu, L. Huang, W. J. Kong, C. Fang, U. Khan, and X. F. Han, Phys. Rev. B **94**, 174434 (2016).

[19] A. van den Brink, G. Vermijs, A. Solignac, J. Koo, J. T. Kohlhepp, H. J. M. Swagten, and B. Koopmans, Nature Commun. **7**, 10854 (2016).

[20] S. Fukami, C. Zhang, Samik DuttaGupta, A. Kurenkov and H. Ohno, Nature Mater. **15**, 535 (2016).

[21] A. Manchon, arXiv:1204.4869.

[22] K. Garello, I. M. Miron, C. O. Avci, F. Freimuth, Y. Mokrousov, S. Blügel, S. Auffret, O. Boulle, G. Gaudin, and P. Gambardella, Nature Nanotech. **8**, 587 (2013).

[23] Z. Z. Sun and X. R. Wang, Phys. Rev. B **74**, 132401 (2006).

[24] J.-Y. Bigot, L. Guidoni, E. Beaurepaire, and P. N. Saeta, Phys. Rev. Lett. **93**, 077401 (2004).

[25] F. Matsukura, Y. Tokura, and H. Ohno, Nature Nanotech. **10**, 209 (2015).

[26] E. Chen, D. Apalkov, Z. Diao, A. Driskill-Smith, D. Druist, D. Lottis, V. Nikitin, X. Tang, S. Watts, S. Wang, S. A. Wolf, A. W. Ghosh, J. W. Lu, S. J. Poon, M. Stan, W. H. Butler, S. Gupta, C. K. A. Mewes, Tim Mewes, and P. B. Visscher, IEEE Trans. Magn. **46**, 1873 (2010).

[27] Recently, there are claims that spin polarization $\hat{s}$ have also a component along $\hat{J} \times \hat{t}$, where $\hat{t}$ is the crystalline direction of the heavy metal, see for example, D. MacNeill *et al.*, Nature Phys. **13**, 300 (2017); A. M. Humphries *et al.*, Nature Commun. **8**, 911 (2017). In this case, one needs only to use $\hat{s} = \hat{J} \times \hat{z}' + a_1 \hat{J} \times \hat{t}$ in Eq. (1), where a_1 is a model parameter. The remaining procedures are similar to what was done in the main text.

[28] X. R. Wang, P. Yan, J. Lu, and C. He, Europhys. Lett. **84**, 27008 (2008).

[29] G. Arfken, *Mathematical Methods for Physicists*, 3rd ed. (Academic Press, Orlando, 1985).

[30] M. d'Aquino, C. Serpico, G. Miano, I. D. Mayergoyz, and G. Bertotti, J. Appl. Phys. **97**, 10E319 (2005).